Synthesis of Silicon-Based Infrared Semiconductors in the Ge−Sn System Using Molecular Chemistry Methods

Jennifer Taraci,[†] S. Zollner,[‡,§] M. R. McCartney,[||] Jose Menendez,[‡] M. A. Santana-Aranda,[‡] D. J. Smith,[‡,||] Arne Haaland,[⊥] Andrey V. Tutukin,[⊥] Grete Gundersen,[⊥] G. Wolf,[†] and J. Kouvetakis*[,†]

Contribution from the Department of Chemistry, Arizona State University, Tempe, Arizona 85287, Center for Solid State Science, Arizona State University, Tempe, Arizona 85287, Department of Physics and Astronomy, Arizona State University, Tempe, Arizona 85287, Motorola Inc., Semiconductor Products Sector, 2200 West Broadway Road, Mesa, Arizona 85202, and Department of Chemistry, University of Oslo, P.B. 1033 Blindern, N-0315 Oslo, Norway

Received June 20, 2001

Abstract: Growth reactions based on a newly developed deuterium-stabilized Sn hydride [$(Ph)SnD_3$] with Ge_2H_6 produce a new family of Ge−Sn semiconductors with tunable band gaps and potential applications in high-speed, high-efficiency infrared optoelectronics. Metastable diamond-cubic films of $Ge_{1-x}Sn_x$ alloys are created by chemical vapor deposition at 350 °C on Si(100). These exhibit unprecedented thermal stability and superior crystallinity despite the 17% lattice mismatch between the constituent materials. The composition, crystal structure, electronic structure, and optical properties of these materials are characterized by Rutherford backscattering, high-resolution electron microscopy, and X-ray diffraction, as well as Raman, IR, and spectroscopic ellipsometry. Electron diffraction reveals monocrystalline and perfectly epitaxial layers with lattice constants intermediate between those of Ge and α-Sn. X-ray diffraction in the $\theta-2\theta$ mode shows well-defined peaks corresponding to random alloys, and in-plane rocking scans of the (004) reflection confirm a tightly aligned spread of the crystal mosaics. RBS ion-channeling including angular scans confirm that Sn occupies substitutional lattice sites and also provide evidence of local ordering of the elements with increasing Sn concentration. The Raman spectra show bands corresponding to Ge−Ge and Sn−Ge vibrations with frequencies consistent with random tetrahedral alloys. Resonance Raman and ellipsometry spectra indicate a band-gap reduction relative to Ge. The IR transmission spectra suggest that the band gap decreases monotonically with increasing Sn fraction. The synthesis, characterization, and gas-phase electron diffraction structure of $(Ph)SnD_3$ are also reported.

Introduction

The spectacular advances in integrated microelectronics over the past 35 years have primarily relied on the unique properties of silicon and its native oxide. Industrial ingenuity combined with key technological breakthroughs has made it possible to double the transistor density in electronic devices about every 2 years. The synthesis of band-gap-engineered epitaxial heterostructures on Si will continue to be important for future generations of high-speed devices. Research and development in this area has focused on the Si−Ge equilibrium system in which complete solubility of the elements allows formation of random $Si_{1-x}Ge_x$ alloys with variable composition, band structure, and lattice constant.[1−3] Recently, synthesis and development of related $Ge_{1-x}Sn_x$ random alloys with similar diamond-cubic structures has attracted considerable attention because of reports that Ge−Sn heterostructures with Sn concentrations up to 15 at. % might exhibit tunable direct band gaps.[4,5] From a synthesis viewpoint, the major problem with Sn incorporation into the tetrahedral Ge lattice is the large (17%) lattice mismatch between the elements and the instability of the diamond-cubic structure of tin (α-Sn) above room temperature.[6] Accordingly, the thermodynamic solubility limit of Sn in Ge is less than 1% while that of Ge in Sn is practically zero.[7] Alloy heterostructures of Ge and Sn are thus unstable, and their synthesis requires conditions that are far from equilibrium.

By using nonequilibrium synthetic methods, progress is being made in growing $Ge_{1-x}Sn_x$ alloys via solid-source molecular beam epitaxy (MBE).[6,8−11] A major challenge facing MBE growth of $Ge_{1-x}Sn_x$ is the propensity of Sn to segregate toward the film surface because of the low surface energy of Sn relative to that of Ge.[12,13] It has been reported that $Ge_{1-x}Sn_x$ films can

[†] Department of Chemistry, Arizona State University.
[‡] Department of Physics and Astronomy, Arizona State University.
[§] Motorola Inc.
[||] Center for Solid State Science, Arizona State University.
[⊥] Department of Chemistry, University of Oslo.

(1) Kasper, E. *Phys. Scr.* **1991**, *T35*, 232.
(2) (a) Bergman, C.; Chastel, R.; Castanel, R. *J. Phase Equilib.* **1992**, *13*, 113. (b) Dismukes, J. P.; Ekstrom, L.; Paff, R. J. *J. Phys. Chem.* **1964**, *68*, 3021.
(3) Jain, S. C. *Germanium−Silicon Strained Layers and Heterostructures*; Academic Press: Boston, MA, 1994.
(4) He, G.; Atwater, H. A. *Phys. Rev. Lett.* **1997**, *79*, 1937.
(5) Ragan, R.; Atwater, H. A. *Appl. Phys. Lett.* **2000**, *77*, 3418.
(6) Gurdal, O.; Desjardins, R.; Carlsson, J. R. A.; Taylor, N.; Radamson, H. H.; Sundgren, J.-E.; Greene, J. E. *J. Appl. Phys.* **1998**, *83*, 162.
(7) *Bull. Alloy Phase Diagrams* **1984**, 5, 266 and references therein.
(8) Fitzgerald, E. A.; Freeland, P. E.; Asom, M. T.; Lowe; W. P.; Macharrie, R. A., Jr.; Weir, B. E.; Kortan, A. R.; Thiel, F. A.; Xie, T.-H.; Sergent, A. M.; Cooper, S. L.; Thomas, G. A.; Kimerling, L. C. *J. Elect. Mater.* **1991**, *20*, 489.
(9) Asom, M. T.; Fitzgerald, E. A.; Kortan, A. R.; Spear, B.; Kimerling, L. C. *Appl. Phys. Lett.* **1989**, *55*, 578.

10.1021/ja0115058 CCC: $20.00
Published on Web 10/16/2001

best be achieved by bombarding the layers with low-energy ions during deposition.[14,15] This process initiates better mixing of the surface and subsurface atoms thereby facilitating incorporation of surface Sn atoms into the growing layer. A major disadvantage is the low thermal stability of MBE-grown Ge−Sn materials.[6,16−18] In some cases, annealing at temperatures as low as 120−300 °C causes Sn precipitation and phase segregation.[6] A plausible explanation is provided by the presence of Sn−Sn vibrations in the Raman spectra which indicate that Sn is not entirely incorporated in the lattice as isolated atoms but also as small aggregates, possibly dimers, trimers, etc. These presumably become the critical nuclei that initiate and facilitate formation of undesirable precipitates even at moderate processing temperatures. One possible source of the Sn clusters in the film might be the molecular beam generated from the Sn Knudsen source which is likely to carry small gas-phase clusters of the element which in turn are incorporated into the film as one unit.

Chemical vapor deposition (CVD) utilizing molecular precursors that incorporate single Sn atoms in the structure should in theory be a suitable route to Ge−Sn materials which contain highly dispersed Sn atoms in isolated tetrahedral sites throughout the diamond-like Ge lattice.[19] Such an arrangement is expected to be thermally more robust than the MBE-grown structures. Until now, there have been no reports to our knowledge of $Ge_{1-x}Sn_x$ crystalline films prepared by chemical methods (CVD) due to lack of suitable sources. The CVD sources that are normally used in industry to deposit silicon-based semiconductors are the classic hydrides SiH_4, GeH_4, Si_2H_6, and Ge_2H_6 and their chlorinated derivatives. The analogous Sn compounds such as SnH_4 and SnH_3Cl are highly unstable at room temperature because of the significantly lower Sn−H bond energy.

In this paper we report the development of a simple Sn hydride derivative that has the necessary thermal stability and volatility to be a viable low-temperature CVD source. The molecular formula is (Ph)SnD_3 (where Ph = C_6H_5 and D = deuterium). Deuterium, the most common, inexpensive, and readily available isotope of hydrogen (other than H), has been previously used to stabilize Sb and Ga hydrides in order to develop practical MOCVD precursors for III−V semiconductors.[20] The deuterium atoms are known to increase the kinetic stability of these molecules. For perdeuterated stannanes such as SnD_4 the enhanced stability provided by D is not yet sufficient, and these compounds decompose at room temperature to form Sn and D_2 gas. However, replacement of one D by Ph in SnD_4 yields (Ph)SnD_3 which has the desired properties, i.e., good thermal stability and volatility (3 Torr at 22 °C), to be a suitable CVD source for Sn. This molecule decomposes at 250 °C in a UHV reactor to form pure Sn via elimination of volatile and thermally robust benzene-d_1 (DC_6H_5) and D_2 byproducts as illustrated by the following equation:

$$(Ph)SnD_3 \rightarrow D_2 + D(Ph) + Sn$$

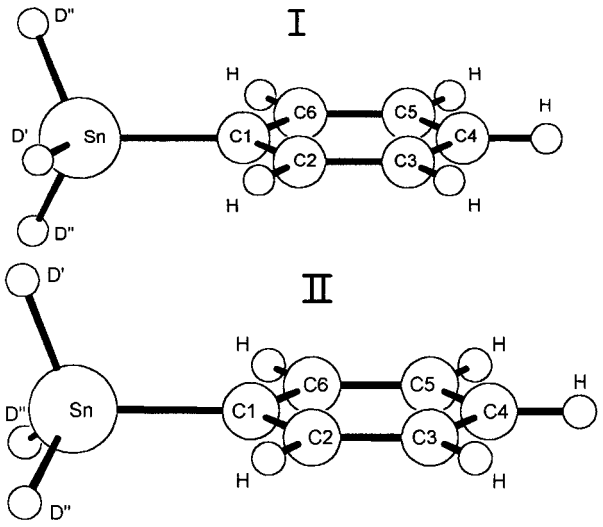

Figure 1. (I) Equilibrium structure of (Ph)SnD_3 obtained by DFT calculations at the B3LYP/LANL2DZ level. (II) Transition state for internal rotation of the SnD_3 group.

This paper describes the synthesis and gas-phase structure of (Ph)SnD_3 as well as reactions of the compound with Ge hydrides to grow highly concentrated $Ge_{1-x}Sn_x$ heterostructures with metastable diamond-cubic structures on Si(100) substrates. These materials display unprecedented thermal stability, superior crystallinity, and unique optical properties.

Results and Discussion

Synthesis and Structure of (Ph)SnD_3. (Ph)SnD_3 is prepared by reaction of the corresponding trichloro(phenyl)stannane with $LiAlD_4$. It is isolated as a colorless liquid that is stable in air for several hours, but longer exposures to atmosphere result in decomposition to produce an unidentified polymeric solid. The title compound was characterized by ^{129}Sn NMR, gas-phase FTIR, and mass spectrometry. Its molecular structure was determined by gas electron diffraction (GED). The mass spectrum shows an isotopic envelope centered at 197 amu as the highest mass peak corresponding to $[(D_{3-x})SnC_6H_5]^+$ ions. The ^{119}Sn NMR spectrum shows a septet centered at −346.15 ppm due to isotopic splitting of the Sn signal by deuterium atoms in the SnD_3 moiety. The ^{13}C and ^{1}H NMR spectra confirmed the presence of the C_6H_5 ring in the structure of (Ph)SnD_3. The IR absorption bands corresponding to the Sn−D modes display the expected isotopic shifts with respect to the Sn−H bands of the normal hydride analogue. The Sn−H and Sn−D stretching modes are observed at 1903, 1883 and 1363, 1355 cm^{-1}, respectively. Peaks corresponding to the C−H stretching modes of the C_6H_5 ring are observed between 3090 and 3015 cm^{-1} in the spectra of both the deuterated and the isotopically pure compounds.

To further characterize (Ph)SnD_3, a determination of the gas-phase structure by gas electron diffraction (GED) was undertaken at the University of Oslo. Structure optimization of (Ph)SnD_3 by density functional theory (DFT) calculations carried out without symmetry restrictions converged to the structure I shown in Figure 1 in which one of the deuterium atoms is lying close to the C_6 ring plane, the dihedral angle τ[C(2)C(1)SnD′] being 4.8°. Bond distances and valence angles are listed in Table

(10) Piao, J.; Beresfor, R.; Licata, T.; Wang, W. I.; Homma, H. *J. Vac. Sci. Technol., B* **1990**, *8*, 221.
(11) Wong, S. S.; He, G.; Nikzad, S.; Ahn, C. C.; Atwater, H. A. *J. Vac. Sci. Technol., A* **1995**, *13*, 216.
(12) Pukite, P. R.; Harwit, A.; Iyer, S. S. *Appl. Phys. Lett.* **1989**, *54*, 2142.
(13) Wegscheider, W.; Olajos, J.; Menczigar, U.; Dondl, U.; Abstreiter, G. *J. Cryst. Growth* **1992**, *132*, 75.
(14) Taylor, M. E.; He, G.; Atwater, H. A.; Polman, A. *J. Appl. Phys.* **1996**, *80*, 4384.
(15) He, G.; Atwater, H. A. *Appl. Phys. Lett.* **1996**, *68*, 664.
(16) Bennett, J. C.; Egerton, R. F. *Vacuum* **1996**, *47*, 1419.
(17) Pukite, P. R.; Harwit, A.; Iyer, S. S. *Appl. Phys. Lett.* **1989**, *54*, 2142.
(18) Zhang, J.; Deng, X.; Swenson, D.; Hackney, S. A.; Krishnamurthy, M. *Thin Solid Films* **1999**, *357*, 85.
(19) Taraci, J.; Tolle J.; McCartney, M. R.; Menendez, J.; Santana, M.; Smith, D. J.; Kouvetakis, J. *Appl. Phys. Lett.* **2001**, *78*, 3607.
(20) Todd, M. A.; Bandari, G.; Baum T. H. *Chem. Mater.* **1999**, *11*, 547.

Table 1. Interatomic Distances (r), Root-Mean-Square Vibrational Amplitudes (l), and Valence and Torsional Angles in $(Ph)SnD_3$ Obtained by Quantum Chemical DFT Calculations and Gas Electron Diffraction[a]

	DFT		GED	
	r_e	l	r_a	l
Distances				
bond dists				
Sn−C	213.3	5.3	213.1(7)	6.1(5)[d]
Sn−D′/D″	171.5/171.6	8.0/8.0	168.6/168.7(14)	8.0/8.0[c]
C(1)−C(2)	141.8	4.6	140.3(2)	4.4(3)[e]
C(3)−C(2/4)	141.0/140.8	4.5/4.5	139.5/139.5(2)	4.4/4.3 (3)[e]
C(2)−H	108.9	7.6	109.9(9)	9.6(12)[f]
C(3/4)−H	108.8/108.8	7.5/7.5	109.8/108.8(9)	9.5/9.5(12)[f]
nonbonded dists				
Sn···C(2/6)	310.6/311.6	8.0	308.6	7.5(7)
Sn···C(3/5)	444.0/444.6	7.3	440.1	8.0(9)
Sn···C(4)	498.1	6.8	493.4	8.7(20)
C(2···C(4/6)	244.1/243.0	5.4/5.5	242.2/242.6	6.1/6.2(5)[d]
C(3)···C(1/5)	246.2/243.4	5.5/5.4	242.3/241.2	6.2/6.2(5)[d]
C(1)···C(4)	284.8	6.1	280.3	6.8(5)[d]
C(2)···C(5)	281.1	6.1	279.2	6.8(5)[d]
Valence Angles				
	$\angle_e$		$\angle_a$	
CSnD′	108.6		113(4)	
CSnD″	110.7, 111.0		115(4)	
C(2)C(1)C(6)	117.9		119.6(8)	
C(1)C(2)C(3)	121.1		119.9(7)	
C(2)C(3)C(4)	120.1		120.5(2)	
C(3)C(4)C(5)	119.6		119.6[c]	
Dihedral Angles				
	τ_e		τ_a	
C(2)C(1)SnD′	4.8		0[c]	
C(2)C(1)SnD″	125.1/−115.2		±120.2[c]	
R-factors[b]			0.047 (50 cm), 0.110 (25 cm), 0.064 (tot.)	

[a] Distances and amplitudes in picometers and angles in degrees. Estimated standard deviations in parentheses in units of the last digit. [b] $R = [\Sigma(w(I_{obs} - I_{calc})^2/\Sigma(wI_{obs})^2]$. [c] Not refined. [d–f] Sets of amplitudes refined with constant differences.

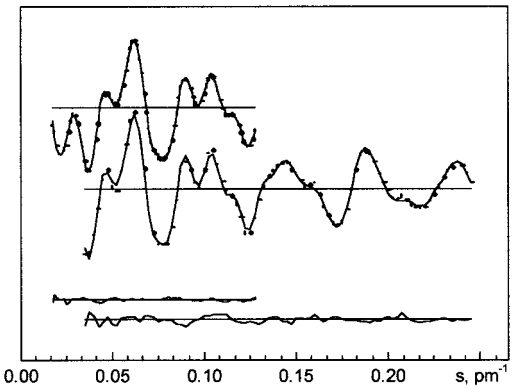

Figure 2. Experimental (dots) and calculated (lines) modified molecular intensity curves of $(Ph)SnD_3$. Below: difference curves.

1. Experimental and calculated intensities are compared in Figure 2, with experimental and calculated radial distribution curves in Figure 3. Calculation of the molecular force field followed by normal coordinate analysis yielded only real vibrational modes, confirming that this C_1 structure corresponds to a minimum on the potential energy hypersurface. When the SnD_3 group was rotated 4.8° to place D′ in the ring plane and the optimization continued under C_s symmetry, the resulting energy was just 7 J mol^{-1} above that of the optimized C_1

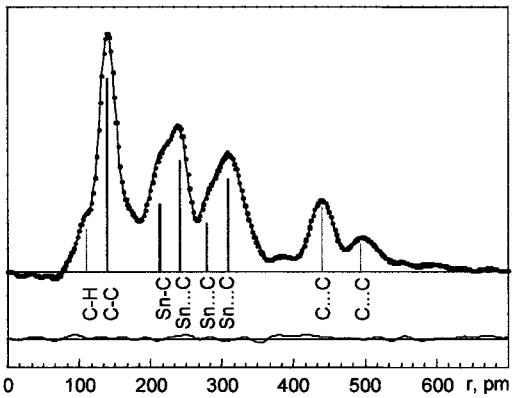

Figure 3. Experimental (dots) and calculated (lines) radial distribution curves of $(Ph)SnD_3$. Below: difference curves. Artificial damping constants $k = 30$ pm^2.

structure. Calculations of the force field and normal coordinate analysis yielded one imaginary frequency, indicating that this C_s model corresponds to a small hump on the potential energy surface, at least at the present computational level. Finally, optimization of another model of C_s symmetry, II (see Figure 1), obtained by rotating the SnD_3 group 30° into an orientation where one Sn−D″ bond is perpendicular to the ring plane, yielded an energy 60 J mol^{-1} above the C_1 equilibrium structure and with one imaginary frequency. Whatever the symmetry of the real equilibrium conformation, the calculations indicate that the barriers to internal rotation of the SnD_3 group are very small.

Least-squares refinement of a molecular model with one deuterium atom in the ring plane and overall C_s symmetry to the GED data yielded structure parameters in good agreement with the calculated; see Table 1. All bond distances and valence angles fall in the expected range. The Sn−C bond distance is not significantly different from that in tetraphenyl stannane, $r_g = 213.7(2)$ pm,[21] and the Sn−D bond distance is indistinguishable from the Sn−H bond distance in SnH_4, $r_0 = 171.1(1)$ pm.[22] It is well-known that introduction of an electropositive substituent to a benzene ring tends to reduce the endocyclic valence angle at the ipso C atom,[23] and the C(2)C(1)C(6) angle is indeed calculated to be 117.9°. The experimental structure is unfortunately too inaccurate to confirm the distortion.

Growth of $Ge_{1-x}Sn_x$ Using $PhSnD_3$. Depositions were carried out in a custom-built ultrahigh-vacuum chemical-vapor deposition (UHV-CVD) system. This is a load-locked hot-wall reactor equipped with a differentially pumped mass spectrometer capable of in situ gas sampling through several micrometer size orifices. Precisely controlled heating of the quartz reactor is provided by a three-zone resistance furnace. The reactor is passivated with a thin Si layer formed by pyrolysis of disilane at 800 °C prior to use. A high-capacity cryopump provides ultrahigh vacuum (1×10^{-9} Torr) before and after each deposition, and a corrosion-resistant turbopump is used during deposition. The single-crystal (100) Si substrates were prepared for deposition in a clean room using a modified RCA process. This method results in formation of an oxide layer of controlled thickness. The substrates were then dipped in 10% HF until their surface became hydrophobic. In a typical experiment, the substrates were loaded into a Si-coated quartz boat, pumped in

(21) Csákvári E.; Shishkov, I. F.; Rozsondai, B.; Hargittai, I. *J. Mol. Struct.* **1990**, *329*, 291.
(22) Kattenberg, H. W.; Oskam, A. *J. Mol. Spectrosc.* **1974**, *51*, 377.
(23) Dominicano, A. In *Stereochemical Applications of Gas-Phase Electron Diffraction, Part B Structural Information for Selected Classes of Compounds*; Hargittai, I., Hargittai, M., Eds.; VCH Publishers: Weinheim, Germany, 1988.

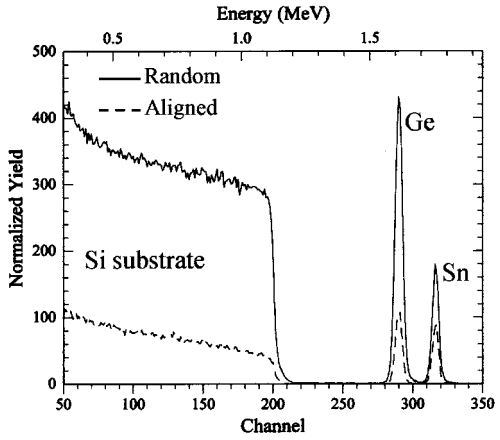

Figure 4. RBS aligned and random spectra for $Ge_{0.88}Sn_{0.12}$. Dechanneling in Sn signal increased with increasing the Sn content in the films.

the load lock to 10^{-6} Torr, and then inserted into the reactor. At this point the pumping was switched to the process turbopump and the temperature was set at 350 °C under a flow of ultrahigh-purity H_2. The appropriate quantities of the reactants were immediately introduced into the reactor, perpendicular to the substrate surface, through separate mass flow controllers which were carefully calibrated for each of the gaseous reactants. The Sn precursor was diluted with a large excess of research grade H_2, and the digermane precursor $(GeH_3)_2$ which was obtained as a 35% mixture in H_2 was used as-received from Voltaix Chemicals.

The reaction of $(GeH_3)_2$ and $(Ph)SnD_3$ at 350 °C on Si(100) resulted in growth of $Ge_{1-x}Sn_x$ samples with concentrations up to 20 at. % Sn. The films adhered extremely well to the substrate, and they were similar in appearance with the Si substrate. Rutherford backscattering (RBS) was used to determine the elemental composition and to detect and identify any possible D, H, or C impurities as well as to estimate the film thickness. The Sn to Ge elemental concentration was obtained by utilizing 2 MeV He^{2+} ions (Figure 4). Forward scattering and carbon resonance [$^{12}C(\alpha,\alpha)^{12}C$] experiments at 4.265 MeV confirmed the absence of deuterium and carbon impurities indicating complete elimination of the Ph and D ligands (the detection limits of C and D using these methods were 0.5% and 1% respectively).

To determine the quality of the epitaxial growth, and to confirm substitutionality of Sn in the Ge diamond-cubic lattice, the random and aligned (channeled) RBS spectra were recorded and compared. Figure 4 shows the two spectra for a sample containing 12% Sn. The most striking feature is that both Sn and Ge atoms channel remarkably well despite the large difference in lattice dimensions between the epilayer and the Si substrate. The channeling of Sn is unique in our CVD grown films and provides unequivocal proof that this element must occupy substitutional sites in the diamond-cubic Ge structure. The extent of substitutionality can be qualitatively assessed by comparing the measured values of χ_{min} (where χ_{min} is the ratio of the aligned vs random peak height) between Ge and Sn in the same sample. This is nearly the same, for both Ge and Sn in a 2 at. % Sn sample and in a 6 at. % Sn sample suggesting that the entire Sn content is substitutional. However, the value of χ_{min} is higher for Sn than Ge in a 12 at. % Sn sample (see Figure 4) meaning that a small fraction of the Sn does not occupy random sites. Since high-resolution transmission electron microscopy and a range of analytical methods including X-ray diffraction (see below) rule out the presence of elemental Sn, we believe that the discrepancy in the channeled spectra is due

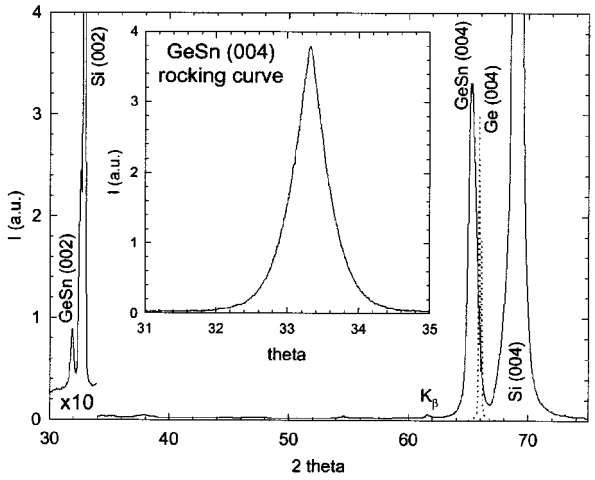

Figure 5. X-ray diffraction data (2θ scan) for Ge−Sn alloy (Sn = 12%) on Si(100). The inset shows a rocking curve of the Ge−Sn(004) peak. Note the presence of the Ge−Sn(002) Bragg reflection which is not typically observed in samples with Sn content lower than 10 at. %. The dotted line shows data for bulk Ge for comparison.

to local ordering of Ge and Sn in random domains within the crystal. Preliminary data from RBS angular scans also point to a possible ordering. Another explanation for the observed dechanneling is a slight distortion of the Sn atoms from their equilibrium tetrahedral positions caused by an increase in structural strain as the Sn content in the alloy increases. The overall χ_{min} for all samples is relatively high compared to the practical limit of about 5% for a perfect Si crystal. This is possibly due to some mosaic spread in the crystal and the presence of misfit dislocations at the interface arising from the lattice mismatch between the Ge−Sn layer and the Si substrate. Nevertheless, the channeling data indicate that the sample is monocrystalline with substantial epitaxial character and relatively few structural defects.

X-ray measurements in the $\theta-2\theta$ mode using a rotating anode generator (50 kV, 200 mA) show a single, strong, and sharp alloy peak corresponding to the (004) reflection of the diamond lattice. In-plane rocking scans of the (004) reflection have a full-width-at-half-maximum of slightly less than 0.5° indicating a tightly aligned spread of crystal mosaics. Similar widths of the rocking curves are found for other relaxed heteroepitaxial films with a large lattice mismatch relative to the substrate. Since there is only one (004) peak from the epilayer in the X-ray data, we conclude that the Sn and Ge are completely mixed and that no phase separation between the GeSn alloy and excess Sn has taken place (no intermetallic compounds with intermediate compositions are reported in the phase diagram).

Finally, it is interesting to note that another X-ray peak emerges for samples with Sn contents higher than about 12 at. %. The peak corresponds to the (002) reflection of the same Ge−Sn crystal lattice, and the intensity increases substantially with increasing Sn content. This reflection is presumably due to the breaking of the inversion symmetry in the zinc blende structure, and it could be related to charge transfer from Sn to Ge. Also, this peak would be expected to appear if the symmetry is broken due to local distortions. One would expect that a Sn atom displaces the Ge nearest neighbors, which would activate the GeSn (002) reflection. This supports local ordering with the Sn atoms perhaps being arranged as second nearest neighbors in the crystal. Figure 5 shows representative X-ray diffraction patterns for a Ge−Sn alloy with 12 at. % Sn.

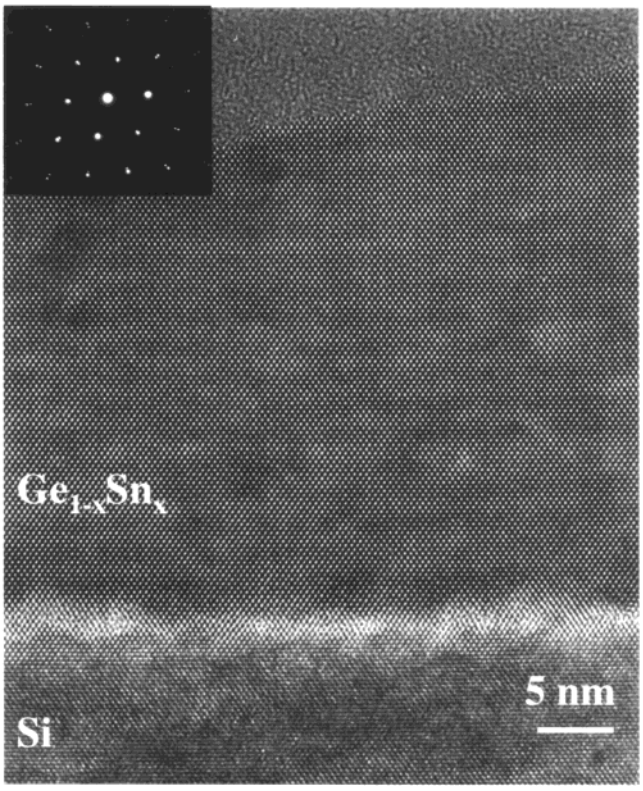

Figure 6. Cross-sectional electron micrographs of $Ge_{0.94}Sn_{0.06}$ showing nearly perfect epitaxy and relatively defect-free coherent growth.

Complementary, cross-sectional transmission electron microscopy revealed that all samples were monocrystalline and heteroepitaxial. Periodic arrays of misfit dislocations and occasional {111} stacking faults originating at the interface were observed but the remainder of the layer was remarkably defect-free. A typical cross-sectional electron micrograph of the interface region demonstrating heteroepitaxial growth of high quality $Ge_{0.94}Sn_{0.06}$ is shown in Figure 6. Selected-area electron diffraction patterns (SAED) confirm that the material has the diamond-cubic structure. There is a marked splitting of the diffraction spots (see Figure 6), even those corresponding to low index planes, confirming the large difference in lattice dimensions between the substrate and the alloy. The lattice parameters obtained from measurements of the SAED patterns from this sample was 5.70 Å which is intermediate to those of pure Ge (5.646 Å) and of the metastable phase of diamond-like α-Sn (6.489 Å). A similar value of 5.696 Å was measured by X-ray diffraction. Optical diffractogram analysis (by Fourier transform of the lattice-fringe images) gave similar values and also showed that the lattice parameter did not vary locally throughout this sample.

Energy-dispersive X-ray microanalysis (EDX) with a probe size smaller than 1 nm was used to determine whether the elemental composition was homogeneous on the nanometer scale and to further verify phase purity. A detailed survey of the compositional profiles in cross-section and plan-view geometries showed that the constituent elements were evenly distributed throughout the sample. Typical elemental profiles, the corresponding line scans, and dark-field images showing the analyzed region of the sample are shown in Figure 7.

To determine the thermal stability of this material, in situ annealing experiments between 350 and 650 °C were made in a high-resolution analytical electron microscope. The sample was heated in the specimen holder for 1 h at increasing 50 °C intervals and then cooled to room temperature for analysis by

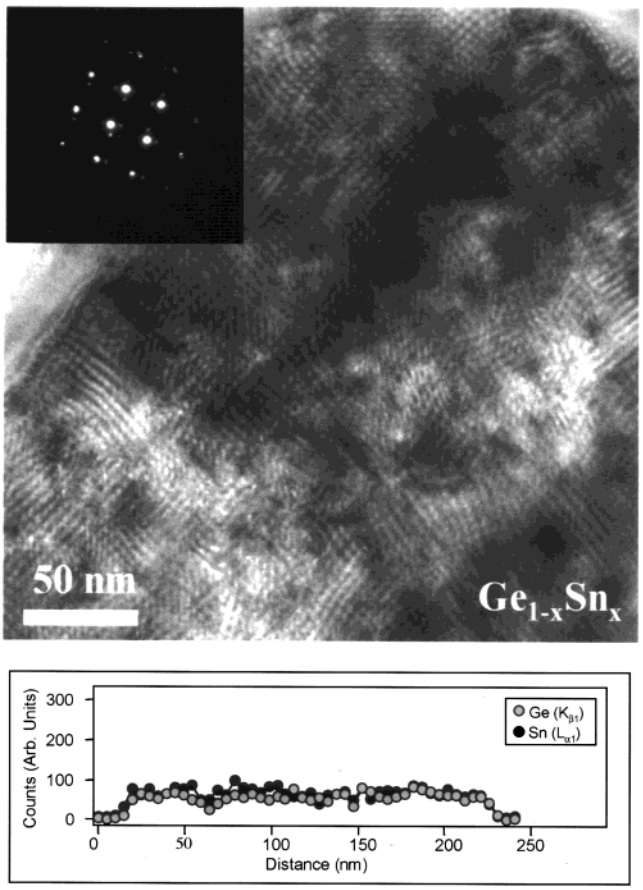

Figure 7. Plan-view electron micrographs of $Ge_{0.95}Sn_{0.05}$ (top) and EDX profile (bottom) showing that the elements are homogeneously distributed throughout the sample.

in situ EDX and electron diffraction. Nanoprobe analysis revealed homogeneous mixing of Sn and Ge, but no Sn precipitation or any other type of phase separation was detected up to about 600 °C. In situ electron diffraction showed that the annealed material remained highly crystalline. This result is in direct contrast to earlier studies of MBE-grown $Ge_{1-x}Sn_x$ films which showed that annealing at temperatures ranging between 100 and 300 °C caused precipitation and Sn segregation particularly toward the film surface.[6]

The higher thermal stability of the CVD grown samples is attributed to the absence of Sn clusters in the films as demonstrated by the complete lack of Sn−Sn lattice modes in Raman spectra (see below). The lack of Sn−Sn bonding and the higher deposition temperatures compared to MBE imply a different growth mechanism for our CVD process. The fact that we deposit at 350 °C compared with −25 to 150 °C for MBE and yet we are able to incorporate Sn into the lattice indicates that the Sn mobility on the surface must be significantly suppressed. This is likely to be due to the presence of large amounts of adsorbed H and D atoms which function as surfactants to slow the surface diffusivity of Sn and thus facilitate incorporation of the atoms into the structure. This process also occurs in CVD of SiGe layers on Si where adsorbed H is well-known to suppress diffusion of Ge and thus promote layer-by-layer growth.[24] In our case, the slightly higher kinetic stability of adsorbed D must make this species a more effective surfactant than H. The net result is complete incorporation of Sn into the lattice rather than surface segregation and absence

(24) Kahng, S.-J.; Ha, Y. H.; Monn, D. W.; Kuk, Y. *Appl. Phys. Lett.* **2000**, *77*, 981.

of Sn clusters and thus an overall increase in thermal stability of the deposited material.

High-resolution electron microscopy of the sample annealed between 600 and 650 °C revealed a distinct variation in morphology and microstructure. The film remained crystalline and heteroepitaxial near the interface. However, the film near the surface was dominated by an array of crystalline and highly coherent islands which seemed to have grown epitaxially from the underlying layer (Figure 8). The lattice fringes of the islands were commensurate with the (111) lattice planes of the layer. Nanoprobe analysis and line scans revealed that the main layer consisted of a uniform distribution of Ge with small concentrations of dissolved Sn. The elemental profile was reversed inside the island, with Sn being in higher concentration (Figure 8). Diffractogram analysis of the lattice fringes revealed a lattice constant for the Sn-rich particles close to that of α-Sn. These results indicate that annealing at 650 °C has caused phase separation with particles near the surface becoming Sn-rich $Sn_{1-x}Ge_x$ alloys with diamond-cubic structure while the bulk layer remained a Ge-rich alloy of the same structure.

High-resolution Raman spectroscopy was used to identify and characterize the local bonding environment of the Sn atoms. The Raman spectrum of the Sn−Ge films was measured using the 488 nm line of an argon laser. Each sample showed a strong peak assigned to Ge−Ge lattice vibrations which is downshifted relative to the Raman peak of pure Ge (Figure 9). A weak peak around 240 cm^{-1} was also observed. Since the Sn−Ge band in Sn-rich Sn−Ge alloys has been observed near 220 cm^{-1} and a higher frequency is expected in Ge-rich alloys, we assign the 240 cm^{-1} peaks to the Sn−Ge vibrations in our sample.[25] The observation of Sn−Ge bands provides strong spectroscopic evidence for the presence of tetrahedral Ge−Sn coordination in our films and supports the formation of an extended random alloy with the diamond-cubic structure. Any additional peaks corresponding to Sn−Sn vibrations were not detected in the Raman spectra, which is consistent with the incorporation of isolated Sn atoms during CVD growth using $(Ph)SnD_3$.

In addition to the structural information obtained from the Raman frequencies, Raman spectroscopy can be used to study the electronic structure of the alloys by measuring the intensity of the Raman peaks as a function of the laser wavelength. In pure Ge, it has been shown that the Raman cross section undergoes a resonant enhancement for laser photon energies near the E_1 and $E_1 + \Delta_1$ gaps. A broad peak about 2.22 eV, halfway between the E_1 and $E_1 + \Delta_1$ transitions, has been measured by Cerdeira et al.[26] Figure 9 shows similar measurements for our $Ge_{0.95}Sn_{0.05}$ alloy and a Ge reference. To extract the Raman cross-section from the measured intensity, a correction must be applied which depends on the dielectric function of the material.[27] Of course, the dielectric function of SnGe alloys is not known. Hence we adopted the following procedure: we rigidly shifted the known dielectric function of pure Ge (see ref 28) to lower energy by an amount ΔE and used the shifted values to compute the correction for the Raman data.[28] The value of ΔE was chosen so that it self-consistently agreed with the shift in the peak of the resonant profile. As seen in Figure 9, we find $\Delta E = 100$ meV. The error in the shift determined from this procedure is probably quite large, but it is apparent that a downshift of the E_1 and $E_1 + \Delta_1$ transitions takes place. Similarly we observe a red shift of the E_2 critical point of about 50 meV from a derivative analysis of spectro-

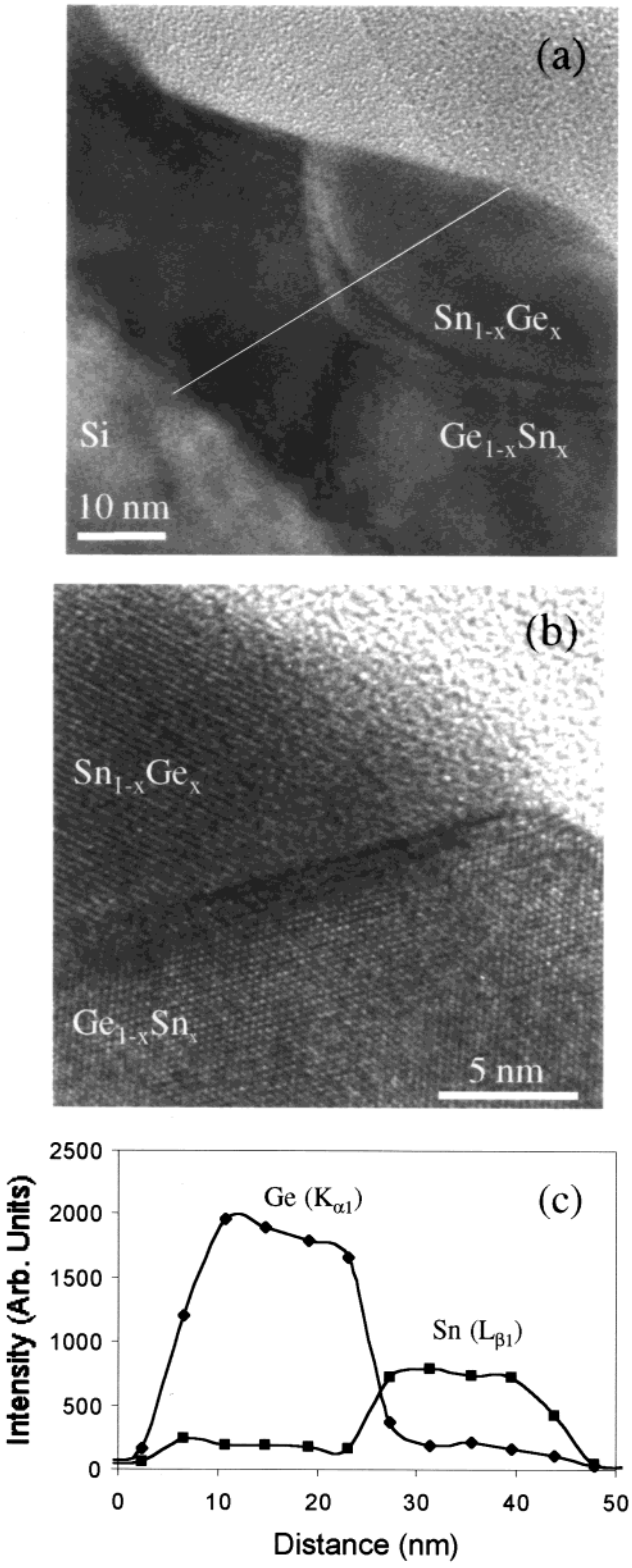

Figure 8. (a) Cross-sectional electron micrograph of $Ge_{0.95}Sn_{0.05}$ annealed at 650 °C showing segregation of an Sn-rich island near the film surface. (a) High-esolution electron micrograph showing lattice fringes of diamond-cubic $Ge_{1-x}Sn_x$ layer and diamond-cubic $Sn_{1-x}Ge_x$ island. (c) EDX elemental profile across the Ge-rich and Sn-rich sections of the layer.

(25) Menéndez, J. Characterization of Bulk Semiconductors using Raman Spectroscopy. In *Raman Scattering in Materials Science*; Weber, W. H., Merlin, R., Eds.; Springer: Berlin, 2000; Vol. 42, p 55.

(26) Cerdeira, F.; Dreyrodt, W.; Cardona, M. *Solid State Commun.* **1972**, *10*, 591.

(27) Richter, W. Resonant Raman Scattering in Semiconductors. In *Springer Tracts in Modern Physics*; Høhler, G., Ed.; Springer-Verlag: Berlin, Heidelberg, New York, 1976; Vol. 78, p 121.

(28) Aspnes, D. E.; Studna, A. A. *Phys. Rev.* **1983**, *B27*, 985.

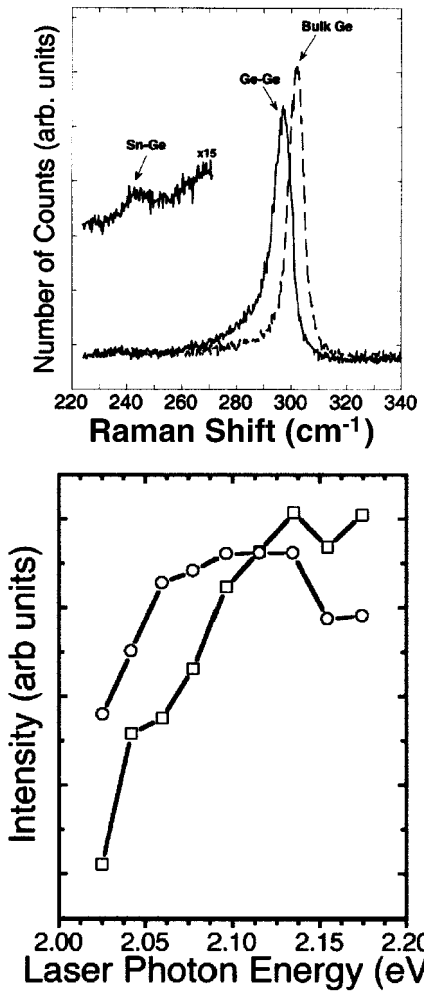

Figure 9. (Top) Raman spectrum showing Ge−Ge and Ge−Sn vibrations of $Ge_{0.95}Sn_{0.05}$. The dotted line shows data for pure Ge for comparison. (Bottom) Excitation profiles for the Raman peak in pure Ge (squares) and the Ge−Ge Raman peak in the $Ge_{0.95}Sn_{0.05}$ alloy (circles). The Raman cross section was extracted from the measured intensities using a correction discussed in the text. The downshift of the resonant maximum for the alloy is attributed to a decrease of the E_1 and $E_1 + \Delta_1$ transition energies as a function of the Sn concentration. This indicates a reduction of valence band−conduction band energy separation in the alloy relative to pure Ge.

scopic ellipsometry data.[29] These data suggest that the band gap of the alloys is also reduced relative to Ge, although it is not possible from this information to determine whether the expected indirect-direct transition has taken place.

This narrowing in band gap prompted us to conduct transmission IR measurements to examine the effect of increasing Sn concentration on absorption. This should provide information of possible band gap variation with composition in the alloy. The transmission spectra of four Ge−Sn films with Sn content ranging from 9 to 18% are shown in Figure 10. The spectrum of the Si substrate is also provided as a reference. Note that the absorption results are very similar for low energies, below the GeSn band gap, and at high energies, above the Si band gap, as expected. However, the transmission drops monotonically with increasing Sn content at intermediate energies. The simplest explanation for these results is a decrease of the band gap of $Ge_{1-x}Sn_x$ as a function of x, since such a reduction is likely to result in increased absorption at a fixed photon energy above the band gap. The data also imply that incorporation of Sn in Ge makes the material a more sensitive infrared photodetector. Further experiments and data analysis aimed toward determination of the absolute band gaps and absorption coefficients are in progress.

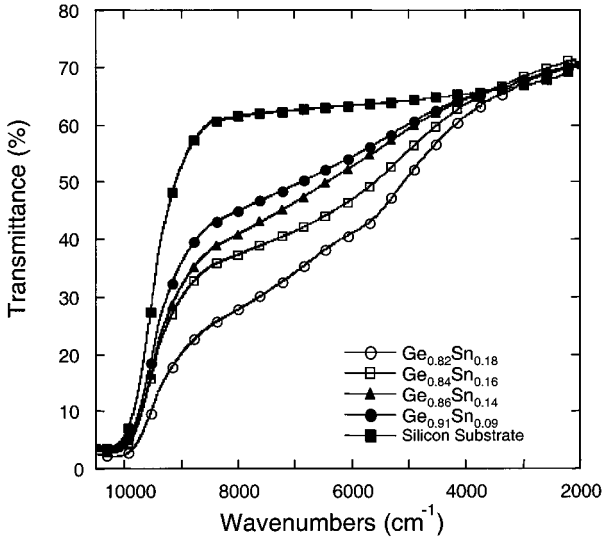

Figure 10. IR transmission spectra of the Si substrate and Ge−Sn samples. At intermediate energies (6000−9000 cm^{-1}) the transmission through the films decreases monotonically indicating that the band gap decreases with increasing Sn concentration.

Concluding Remarks

We have developed for the first time a molecular method to deposit highly concentrated semiconductors in the Ge−Sn alloy system with tunable band gaps in the infrared. Transmission FTIR measurements of layers grown on Si show that transmission decreases (absorption increases) monotonically with increasing Sn content indicating that the band gap of the alloys decreases with increasing Sn fraction. Our synthetic approach is based on reactions of a newly prepared deuterium-stabilized Sn hydride, $(Ph)SnD_3$. This compound is designed to have the necessary volatility and reactivity to interact at low temperatures with common reagents such as $(GeH_3)_2$ to yield pure products via elimination of extremely stable gaseous byproducts, including benzene, hydrogen, and deuterium. This method is currently applied to explore formation and systematic structural characterization of a wide range of concentrations across the entire Sn−Ge compositional range. This includes growth of epitaxial alloys on suitable substrates and buffer layers that are predicted to have direct band gaps.

Experimental Section

Synthesis $(Ph)SnD_3$. A solution of $(Ph)SnCl_3$ (10 g, 33 mmol) in 20 mL of ethyl ether was added, dropwise, to a solution of $LiAlD_4$ (3.5 g, 83 mmol) in 150 mL of ethyl ether which was cooled to −70 °C. The resulting solution was stirred for 30 min at −70 °C and at −20 °C for an additional 60 min during which time the solution turned to a dark brown mixture. The mixture was filtered under N_2, and a clear filtrate was isolated and separated by distillation. The volatiles from the filtrate were passed through traps held at −20 and −196 °C which retained $(Ph)SnD_3$ (2 g, 10 mmol, 30% yield) and ether, respectively. $(Ph)SnD_3$ has a vapor pressure of 2−3 Torr at 22 °C.

IR (gas phase): 3079 (w), 3067 (w), 3025 (w), 1363 (m), 1355 (st), 726 (w), 691 (w), 489 (vst), 458 (w) cm^{-1}. ^{119}Sn NMR [toluene-d_8, referenced to $Sn(CH_3)_4$]: −346.15 ppm (sept, $J = 294$ Hz, SnD_3). The seven peaks observed due to isotopic splitting from deuterium are −350.87, −348.25, −347.72, −346.15, −344.57, −342.99, and

(29) Junge, K. E.; Lange, R.; Dolan, J. M.; Zollner, S.; Dashiell, M.; Orner, B. A.; Kolodzey, J. *Appl. Phys. Lett.* **1996**, *69*, 4084. Vina, L.; Hochst, H.; Cardona, M. *Phys. Rev. B* **1985**, *31*, 958.

−341.41 (ppm). EIMS (*m*/*e*): isotopic envelopes centered at 120 (DSn^+), 197 ($DSnC_6H_5^+$), and 78 ($C_6H_6^+$). For comparison (Ph)SnH_3 was prepared using the same procedure described above for the (Ph)-SnD_3 analogue. IR (gas phase): 3087 (w), 3067 (w), 3013 (w), 1903 (m), 1883 (m), 726 (w), 687 (s), 691 (w), 505 (w), 469 (w).[30] The peaks corresponding to Sn−H stretching and bending vibrations display the calculated isotopic shifts with respect to those for (Ph)SnD_3.

Gas-Phase Structure. The structure of $PhSnD_3$ was optimized using the GAUSSIAN program package, the B3LYP functional, and a standard LANL2DZ basis.[31] Molecular force fields were scaled as described in ref 32 and transferred to the program ASYM40 for calculation of root-mean-square amplitudes of vibration and vibrational correction terms, $D = r_e - r_a$, at the temperature of the electron diffraction experiment.[33] The gas electron diffraction pattern was recorded on the Baltzers KDG2 unit at the University of Oslo[34] with a metal inlet system at 22 °C. Exposures were made at nozzle-to-plate distances of about 25 cm (3 plates) and 50 cm (3 plates) using the BAS 1800 II imaging plates of Fuji. The plates were scanned on a BAS 1800 II imaging plate reader and the intensity data processed using a program written by S. Samdal, D. Shorokhov, and T. G. Strand. Atomic scattering factors were taken from ref 35. Backgrounds were drawn as least-squares adjusted polynomials to the difference between the total experimental intensity and the calculated molecular intensity, and the molecular structure was refined by least-squares calculations on the intensity data using the program KCED 26 written by G. Gundersen, S. Samdal, H. M. Seip, and T. G. Strand.

Inspection of the equilibrium structure obtained by DFT optimization of $PhSnD_3$ without imposition of symmetry showed that the (Ph)Sn fragment adheres closely to C_{2v} symmetry, the deviation in bond distances being less than 0.1 pm and that in angles less than 0.1°. Similarly the SnD_3 fragment was found to approach C_s symmetry. Least-squares structure refinement to the GED data were therefore based on a model of C_s symmetry in which one Sn−D bond is lying in the ring plane. Six independent structure parameters were refined. The first four were the following: (i) the Sn−C bond distance; (ii) a common scale factor for the three symmetry-inequivalent C−C bond distances (each C−C bond distance assumed to be equal to the calculated bond distance multiplied by this scale factor); (iii) a common scale factor for the three symmetry-inequivalent C−H bond distances; (iv) a common scale factor for the two symmetry-inequivalent Sn−D bond distances. After the C−C bond distances have been fixed, the structure of the C_6 ring is determined by two valence angles, e.g. the C(2)C(1)C(6) and C(3)C-(4)C(5) valence angles. The former was refined as an independent parameter, the latter was fixed at the calculated value. The last structure parameter to be refined was the CSnD angle.

In addition to the six structure parameters we refined six vibrational amplitudes as indicated in Table 1. Nonrefined amplitudes were fixed at the calculated values. Introduction of vibrational correction terms (*D*) led to considerably poorer fit between calculated and experimental intensities. The refinements were therefore carried out on a geometrically consistent r_a structure. The refinements proceeded without difficulties to yield the best values listed in Table 1. The estimated standard deviations have been multiplied by a factor of 2.0 to include added uncertainty due to data correlation and further expanded to include an estimated scale uncertainty of 0.1%.

Acknowledgment. The work at ASU was supported by the National Science Foundation (Grant DMR-9902417) and the Army Research Office (ARO). We are grateful to the Norwegian Research Council (Program for Supercomputing) for a grant of computer time. M.A.S.-A. acknowledges partial support from CONAC y T-Mexico.

JA0115058

(30) Kuivila, H. G.; Beumel, O. F. *J. Am. Chem. Soc.* **1961**, *83*, 1246.
(31) Frisch, M. J.; Trucks, G. W.; Schlegel, H. B.; Scuseria G. E.; Robb, M. A.; Cheeseman, J. R.; Zakrzewski, V. G.; Montgomery, J. A., Jr.; Stratmann, R. E.; Burant, J. C.; Dapprich, S.; Millam, J. M.; Daniels, A. D.; Kudin, K. N.; Strain, M. C.; Farkas, O.; Tomasi, J.; Barone, V.; Cossi, M.; Cammi, R.; Mennucci, B.; Pomelli, C.; Adamo, C.; Clifford, S.; Ochterski, J.; Petersson, G. A.; Ayala, P. Y.; Cui, Q.; Morokuma, K.; Malick, D. K.; Rabuck, A. D.; Raghavachari, K.; Foresman, J. B.; Cioslowski, J.; Ortiz, J. V.; Baboul, A. G.; Stefanov, B. B.; Liu, G.; Liashenko, A.; Piskorz, P.; Komaromi, I.; Gomperts, R.; Martin, R. L.; Fox, D. J.; Keith, T.; Al-Laham, M. A.; Peng, C. Y.; Nanayakkara, A.; Gonzalez, C.; Challacombe, M.; Gill, P. M. W.; Johnson, B.; Chen, W.; Wong, M. W.; Andres, J. L.; Gonzalez, C.; Head-Gordon, M.; Replogle, E. S.; Pople, J. A. *Gaussian 98*, revision A.7; Gaussian, Inc.: Pittsburgh, PA, 1998.
(32) Scott, A. P.; Radom, L. *J. Phys. Chem.* **1996**, *100*, 16502.
(33) Hedberg, L.; Mills, I. M. *J. Mol. Spectrosc.* **1993**, *160*, 117.
(34) Zeil, W.; Haase, J.; Wegmann, L. *Z. Instrumentenkd.* **1966**, *74*, 84.
(35) Ross, A. W.; Fink, M.; Hilderbrandt, R. L. In *International Tables for Crystallography*; Kluwer Academic Publishers: Dordrecht, The Netherlands, 1992; Vol. C, p 245.